

## Variogram analysis of helicopter magnetic data to identify paleochannels of the Omaruru River, Namibia

Stefan Maus\*, K. P. Sengpiel‡, B. Röttger‡, B. Siemon‡, and E. A. W. Tordiffe\*\*

### ABSTRACT

The geomagnetic field over sedimentary basins is very sensitive to variations in basement depth. Therefore, magnetic surveys are widely used to map basement topography in petroleum and groundwater exploration. We propose variogram analysis as a more accurate alternative to power spectral methods. Data variograms are computed from aeromagnetic flight-line data. To estimate depth, the data variograms are compared with model variograms for a range of source depths. We use the exact space domain counterparts of a fractal power spectral model as model variograms. To demonstrate the utility of this method for groundwater exploration, we map the basement topography of the Omaruru Alluvial Plains in Namibia. A comparison with electromagnetic (EM) resistivities and drilling information confirms the high accuracy—but also the limitations—of variogram analysis depth. Variogram analysis makes maximum use of short-wavelength contributions to the magnetic signal, which is the key to the resolution of shallow basement topography. Moreover, by using a realistic source model and avoiding extensive data preconditioning and the transform to wavenumber domain, variogram analysis is likely to provide improved magnetic depth estimates even for deep basins.

### INTRODUCTION

Because of the instability of magnetic minerals in oxidizing environments, the magnetization of sediments is usually weak compared with the magnetization of the crystalline basement. In this case, the crystalline basement is equivalent to the magnetic basement, being defined as the uppermost occurrence of rocks carrying a significant magnetization.

$\Delta T$  magnetic maps are the smoother the greater the height of the observation plane above the magnetic basement. This effect is quite prominent, as illustrated in Figure 1. The smoothness/ruggedness of the magnetic field is reflected in its power spectrum  $P(\mathbf{s})$ , where  $\mathbf{s}$  is the 2-D horizontal wavevector. The higher the relative power for small wavenumbers  $|\mathbf{s}|$ , the more rugged the appearance of the field. The power  $P(\mathbf{s})$  of the magnetic field in the observation plane is related to the power of the field at basement level  $P_0(\mathbf{s})$  by

$$P(\mathbf{s}) = P_0(\mathbf{s})e^{-2z|\mathbf{s}|}, \quad (1)$$

where  $z$  is the depth to the basement, hence, the parameter of interest. To obtain  $z$  from equation (1), we require a model for the power spectrum  $P_0(\mathbf{s})$  of the field at basement level. Assuming that the  $e^{-2z|\mathbf{s}|}$  term dominates the shape of the power spectrum, spectral slope methods (Spector and Grant, 1970) are based on the implicit assumption  $P_0 \equiv \text{constant}$ . Hahn et al. (1976) propose subtracting 10% from these white depths for a more reliable depth estimate. A breakthrough in our understanding of magnetic power spectra was the finding that the magnetic field at source level is self-similar (fractal) and can be described by a model  $P_0(\mathbf{s}) \propto |\mathbf{s}|^{-\gamma}$ , with  $\gamma \approx 3$  (Gregotski et al., 1991; Pilkington and Todoeschuck, 1993). To correct for self-similar source, Pilkington et al. (1994) suggest dividing the power spectrum by  $|\mathbf{s}|^{-3}$  before applying a spectral slope method. However, even with this correction, depth estimates remain unreliable (Maus and Dimri, 1996) for several reasons.

For spectral analysis the magnetic flight-line data must be transformed to a regular grid. Since data density is typically 50 times higher along- than across-line, gridding invariably leads to a loss of information. Furthermore, gridded data are likely to be smoother than the actual magnetic field. The subsequent steps—making the grid periodic, fast Fourier transform, and azimuthal averaging—again lead to distortions in the power spectrum.

Manuscript received by the Editor September 24, 1996; revised manuscript received September 18, 1998.

\*Institut für Geophysik und Meteorologie der Technischen Universität Braunschweig, Mendelssohnstr. 3, 38106 Braunschweig, Germany. E-mail: smaas@gwdg.de.

‡Bundesanstalt für Geowissenschaften und Rohstoffe, Stilleweg 2, D-30655 Hannover, Germany. E-mail: heli@bgr.de.

\*\*Department of Water Affairs, Private Bag 13193, Windhoek, Namibia.

© 1999 Society of Exploration Geophysicists. All rights reserved.

Power spectrum estimation can be avoided altogether by transforming a model power spectrum analytically to the space domain. This approach is intuitively appealing because it means carrying the model without loss of information toward the data instead of the data toward the model. This difference in approach is illustrated in Figure 2. A spectral analysis in the wavenumber domain (left side) can be substituted by an equivalent autocorrelation analysis (middle) or a variogram analysis (right side) in the space domain. Whether it is better to use the autocorrelation function (ACF) or the variogram depends on the statistical nature of the data. As discussed in Maus (1999, this issue), magnetic and gravity data are better described by variograms than by ACFs.

Here, we demonstrate the utility of the variogram analysis method (Maus, 1999) on helicopter magnetic data of the Omaruru Alluvial Plains in Namibia. First, we describe the

spectral model, which is based on simplifying assumptions regarding the distribution of magnetization in the crust. Although these assumptions are common to a variety of magnetic methods, it is worthwhile to repeat them here. The use of a spectral model in terms of an equivalent variogram analysis is outlined in the following section. After introducing the survey area, we illustrate different statistical methods of estimating depth on two sample areas. We then compare the variogram analysis depths for the whole survey area with the electromagnetic (EM) resistivities to verify the boundary of the alluvial deposits. A comparison of basement reliefs derived by variogram analysis and an automated spectral slope method illustrates the improvements possible with the new method. Finally, we verify basement depth with drilling results, finding a reasonable agreement.

**SPECTRAL MODEL**

To derive a realistic model for  $P_0(s)$  in equation (1), one must make assumptions on the statistical distribution of magnetization in the basement rock. The magnetization  $\mathbf{M}(\mathbf{r})$  at a location  $\mathbf{r}$  is the vector sum of the induced magnetization  $\mathbf{M}_i(\mathbf{r})$  and the remanent magnetization  $\mathbf{M}_r(\mathbf{r})$ . The magnetization  $\mathbf{M}_i(\mathbf{r})$ , induced by the geomagnetic field  $\mathbf{N}(\mathbf{r})$ , can be written as

$$\mathbf{M}_i(\mathbf{r}) = \bar{\mathbf{X}}(\mathbf{r})\mathbf{N}(\mathbf{r}), \tag{2}$$

where  $\bar{\mathbf{X}}(\mathbf{r})$  is a 3-D susceptibility tensor. If we assume isotropic susceptibility  $\bar{\mathbf{X}}(\mathbf{r}) = \chi(\mathbf{r})\mathbf{I}$ , where  $\mathbf{I}$  is the identity matrix, and a constant inducing geomagnetic field  $\mathbf{N}(\mathbf{r}) \equiv \mathbf{N}_0$ , equation (2) simplifies to

$$\mathbf{M}_i(\mathbf{r}) = \chi_i(\mathbf{r})\mathbf{N}_0. \tag{3}$$

Here,  $\chi_i(\mathbf{r})$  is the susceptibility that one would measure from a rock sample in a laboratory.

While induced magnetization can be described by a scalar susceptibility  $\chi_i(\mathbf{r})$ , remanent magnetization is a true vector field. However, to arrive at a simple statistical model, we have to assume that any nonnegligible remanent magnetization is aligned with the normal field. Then, remanent magnetization can be described by

$$\mathbf{M}_r(\mathbf{r}) = \chi_r(\mathbf{r})\mathbf{N}_0, \tag{4}$$

similar to the induced magnetization. Possible consequences of this simplifying assumption are discussed in point 2 of the "Limitations" section. Combining equations (3) and (4), the magnetization  $\mathbf{M}(\mathbf{r})$  can be expressed as

$$\mathbf{M}(\mathbf{r}) = [\chi_i(\mathbf{r}) + \chi_r(\mathbf{r})]\mathbf{N}_0 = \chi_{i+r}(\mathbf{r})\mathbf{N}_0 \tag{5}$$

in terms of an apparent scalar susceptibility distribution  $\chi_{i+r}(\mathbf{r})$  in the basement rock. In the next step, a statistical expression for  $\chi_{i+r}(\mathbf{r})$  has to be found.

Recent studies suggest that the susceptibility distributions  $\chi_i(\mathbf{r})$  and  $\chi_r(\mathbf{r})$  in the earth's crust are self-similar (Pilkington and Todoeschuck, 1993; Pilkington et al., 1994; Maus and Dimri, 1995). A characteristic of self-similar random functions is that their power spectrum  $P(\mathbf{k})$  is proportional to a power of the wavenumber  $\mathbf{k}$ , namely  $P(\mathbf{k}) \propto |\mathbf{k}|^{-\beta}$ , where  $\beta$  is a variable scaling exponent. A self-similar distribution of the susceptibility  $\chi_{i+r}(\mathbf{r})$  in the basement rock causes a self-similar magnetic field immediately above the basement (Pilkington and

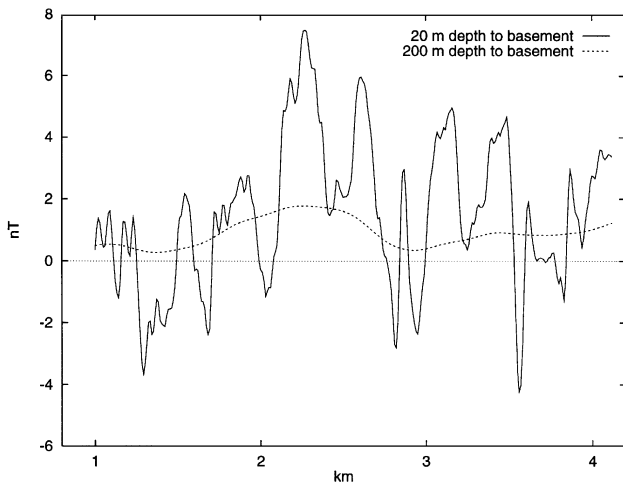


FIG. 1. Synthetic  $\Delta T$  magnetic data on profiles at different heights above a level basement model with self-similar magnetization. To eliminate edge effects the profiles of 3 km length are located over the center of a larger  $5 \times 5$ -km model.

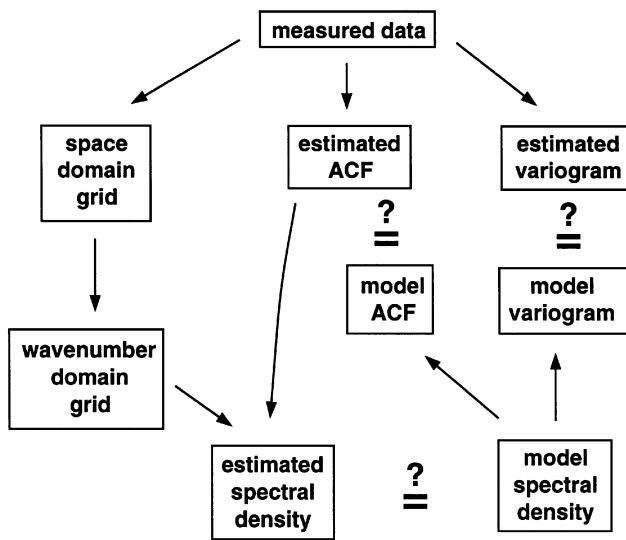


FIG. 2. The different possibilities of using a spectral model to invert magnetic data.

Todoeschuck, 1993; Maus and Dimri, 1995). In combination with equation (1), this leads to a spectral model

$$P_{\Delta T}(\mathbf{s}) = c_s \left( \frac{\mu_0}{2N} \right)^2 B[1/2, (\beta + 1)/2] \times \underbrace{\left( n_z^2 + H^2 \cos^2 \theta \right)^2}_{Dir(\theta)} s^{-\beta+1} \exp(-2sz) \quad (6)$$

for the  $\Delta T$  magnetic field in a horizontal observation plane [Maus, 1999, equation (6)]. Here,  $\mathbf{s}$  is the horizontal wavevector,  $c_s$  is the intensity of susceptibility variations,  $\mu_0$  is the magnetic permeability of vacuum,  $\mathbf{N}$  is the vector of the geomagnetic field,  $B$  is the beta function  $B(x, y) = \Gamma(x)\Gamma(y) / \Gamma(x + y)$ ,  $Dir(\theta)$  describes the anisotropy of the power spectrum as a function of the angle  $\theta$  between the horizontal field component  $\mathbf{H}$  and the wavevector  $\mathbf{s}$ ,  $\beta$  is the 3-D scaling exponent of the susceptibility distribution  $\chi_{i+r}(\mathbf{r})$  in the basement rock, and  $z$  is the height of the observation plane above the magnetic basement.

**MAGNETIC DEPTH**

As illustrated in Figure 2, inversion of a magnetic data set using a spectral model can be carried out in several different ways. Earlier spectral analysis methods pursued the left path in Figure 2. Depth was estimated from linear sections in the power spectrum (Spector and Grant, 1970). There was no analytical expression for the entire power spectrum which could have been shifted to the space domain. Depth therefore had to be estimated in the wavenumber domain. In contrast, equation (6) provides a model for the entire 2-D magnetic power spectrum. This spectral model has an exact variogram counterpart in the space domain, which is obtained by the integral transform (Yaglom, 1986, p. 435).

$$V(\mathbf{d}) = \int_{-\infty}^{\infty} \int_{-\infty}^{\infty} [1 - \cos(\mathbf{d} \cdot \mathbf{s})] P_{\Delta T}(\mathbf{s}) du dv, \quad (7)$$

where  $\mathbf{s} = (u, v)$  is the horizontal wavevector and  $\mathbf{d}$  is the corresponding vector separation in the space domain. A variogram  $V(\mathbf{d})$  depicts the expected square of the difference between two data values as a function of their vector separation  $\mathbf{d}$ . With equation (7) a spectral analysis in the wavenumber domain using equation (6) can be substituted by an equivalent variogram analysis in the space domain. Hence, instead of computing and interpreting power spectra, we analyze variograms. The most important advantage is that variograms can be estimated directly from the flight-line data, making use of their higher along-line resolution as compared to grids. Furthermore, computing variograms is simple and straightforward. Variograms are also easier to understand than power spectra, reducing the risk of misinterpretation.

The model variogram defined by equations (6) and (7) is governed by three unknowns:  $z$ ,  $c_s$ , and  $\beta$ . A smooth magnetic field may be caused either by a great depth to source  $z$  or a smooth distribution of basement magnetization reflected in a high value of  $\beta$ . Because of this trade-off, only one of the parameters  $z$  and  $\beta$  can be resolved at a time. In areas without major changes in the geology of the basement, it is reasonable to assume a constant scaling exponent of the susceptibility distribution (Maus and Dimri, 1995). For the purpose of deriving

a relief of the magnetic basement, the optimum values of  $z$  and  $c_s$  are estimated from the variograms, keeping  $\beta$  constant. A lower scaling exponent  $\beta$  leads to greater depth estimates, and vice-versa (Maus and Dimri, 1996). Thus, depth estimation can be calibrated by choosing the constant scaling exponent in such a way that the inversion yields the average sensor altitude for data over outcropping basement.

The optimum values for  $z$  and  $c_s$  are obtained by inversion. An appropriately sized window is moved over the magnetic data set, as illustrated in Figure 3. Plots of model variograms for different values of  $z$  indicate that the window size must be at least five times the maximum depth to be resolved (Maus, 1999, Figure 5). The accuracy of depth estimates increases with window size, while the lateral resolution decreases. From our experience, a window size of around twenty times the maximum depth is a good compromise between lateral resolution and accuracy of depth for survey areas with shallow basement. For each position of the window, the variogram of the data within the window is computed and compared with model variograms for a range of  $z$  values. The model variograms can be computed beforehand to save computing time. The best-fitting model variogram provides an estimate for the depth to basement. To focus the analysis on the present window position, a linear trend is removed from the magnetic data of each flight-line section before computing its variogram. The model variograms are modified accordingly. Details of this detrending are discussed in Maus (1999). We utilize only 1-D along-line variograms, averaged over adjacent flight lines. In principle, a 2-D variogram could be computed from the flight-line data within each window. However, the 2-D variograms of magnetic data are anisotropic, and an analytical solution to the integrals in equation (7) does not exist. Apart from the numerical difficulties of a 2-D variogram analysis, accuracy may also be affected by line-leveling errors. In contrast, the 1-D variogram analysis does not require any line leveling.

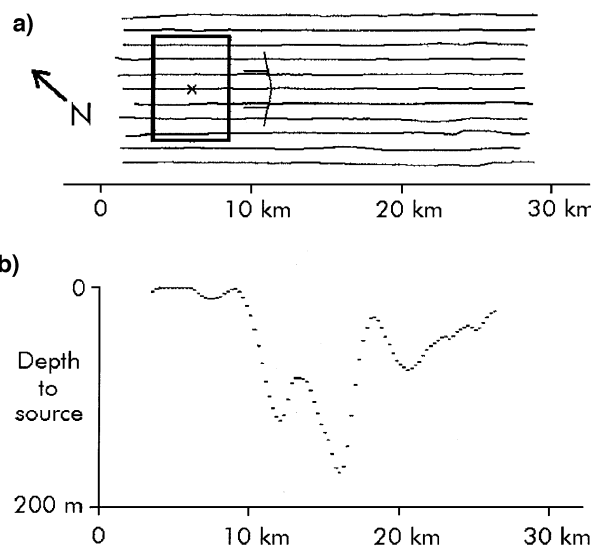


FIG. 3. A window is moved over the survey area (a). For each window position the variograms of the intersecting flight lines are computed. The mean variogram is then compared with model variograms to find the optimum depth in a least-squares sense. Consecutive depth estimates are plotted here as a profile (b).

From our experience, variograms of magnetic data have  $\lim_{d \rightarrow 0} V(d) = 0$ , and the main depth information is contained in low lags. This motivates using a misfit function

$$\text{misfit} = \sum_i [\ln V_{est}(\tau_i) - \ln V_{model}(\tau_i)]^2 \quad (8)$$

for optimizing depth. Before processing a survey, the assumption  $\lim_{d \rightarrow 0} V(d) = 0$  should be verified by examining the variograms of sample areas. If the assumption does not hold, equation (8) may have to be modified.

### Limitations

Following is a list of the known sources of error in variogram analysis depth. These limitations arise primarily from the inherent nonuniqueness of the magnetic inverse problem. Similar problems can therefore be expected with all magnetic depth estimation methods.

- 1) Nonuniqueness between greater source depth and smoother source distribution leads to a trade-off between  $z$  and  $\beta$ . The necessary assumption of  $\beta = \text{constant}$  could be violated by changes in basement lithology.
- 2) Nonuniqueness of depth versus direction of magnetization is summarized in Table 1. A north-south profile at the magnetic equator over an induced magnetic source carries stronger texture than a profile in the east-west direction (hence, the well-known recommendation to fly north-south rather than east-west at low magnetic latitudes). The smoothness of an east-west profile corresponds to the smoothness of a north-south profile at almost twice the altitude above basement. At the magnetic equator, a depth estimate of 98 m from a north-south profile could actually be caused by a basement at 52 m depth carrying an east-west remanent magnetization. Hence, strong horizontal remanent magnetizations are a potential source of error.
- 3) Magnetic anomalies caused by basement topography cannot be distinguished from anomalies resulting from intrabasement magnetization contrasts. For example, this can lead to overshooting depth estimates at steep topographic gradients. The ensuing topographic magnetic anomaly constitutes a long-wavelength feature, increasing the long-to-short-wavelength power ratio and leading to overestimated source depth.
- 4) Care must be taken to eliminate time variations of the magnetic field. Noisy sections of the flight-line data must be excluded from the analysis because they bias depth toward smaller values.

**Table 1. Variogram analysis depth estimates from a real data variogram. Estimated depth strongly depends on the assumed direction of basement magnetization. For example, a magnetic profile over a vertically magnetized basement (incl. = 90°) at 84 m depth is as smooth as a profile over a basement at 52 m depth with horizontal magnetization perpendicular to the profile direction (incl. = 0°, decl. = 90°).**

		Declination		
		0°	16°	90°
Inclination	0°	98 m	96 m	52 m
	64°	86 m	86 m	81 m
	90°	84 m	84 m	84 m

- 5) Surface or intrasediment magnetizations obviously reduce depth estimates.

### FIELD EXAMPLE

In line with the agreement on technical cooperation between Namibia and Germany, an area of 100 × 26 km was surveyed by airborne geophysics to identify proposed groundwater-bearing paleochannels of the Omaruru River (Figure 4). The helicopter survey was flown at constant terrain clearance, the magnetic sensor at approximately 60 m and the EM system at 40 m above terrain.

**Geology.**—The stratigraphy of the test study area in Namibia (Bittner et al., 1994) (Figure 5) can be subdivided into two major components: (1) the older Damara Sequence (Late Proterozoic) comprising granitic, quartzitic, and quartz-mica schist lithologies, intruded by mainly northeasterly trending dolerite dikes of Triassic age, and (2) the overlying alluvial deposits of Kalahari age (Tertiary to Recent). These so-called Omaruru Alluvial Plains (OMAP) were the target for groundwater exploration (Nawrowski, 1993). The OMAP drainage basin has been involved in tectonic movements since Tertiary times; one faulting event has been dated at Middle to Late Pleistocene or Recent. Seismic activity along two sets of Landsat lineaments, one of which is parallel to the predominant northeasterly direction of Damara faults, suggests that processes of faulting and uplifting are still active (Bittner et al., 1994).

The southeasterly displacement of Omaruru drainage paths was probably tectonically induced. Channels have a tendency to migrate down tectonic tilt (Leeder and Alexander, 1987). Variations in channel discharge because of sea level change and variations in sedimentary recharge because of climatic change could have been further reasons for channel migration (Alexander et al., 1994).

**The  $\Delta T$  and  $c_s$  magnetic maps.**—The total field anomaly map of the survey area is shown in Figure 6. Using variogram analysis, we estimated the source intensity  $c_s$  from the  $\Delta T$  flight-line data using a 500-m window along single lines and further assuming  $\beta \equiv 2.6$  and  $z = \text{terrain clearance}$ . This high-resolution  $c_s$  intensity map is shown in Figure 7. The  $c_s$  map provides superior near-surface resolution of magnetic source, since  $c_s$  is estimated from very short along-line  $\Delta T$  variations—exactly the short-wavelength information lost in gridding  $\Delta T$  data. The  $c_s$  map is easy to interpret. In contrast to  $\Delta T$ ,  $c_s$  is high when magnetization is high and low when magnetization is low.

### Magnetic depth from two sample areas

To illustrate the spectral methods discussed above, we have selected two sample areas of 5 × 20 km (Figure 6). The first area has outcropping basement, while the second area is situated over the center of one of the main paleochannels. From the drilling results discussed below, the depth to basement in the center of the second area is around 200 m but is probably shallower at its sides.

**Depth from the spectral slope.**—By previous spectral analysis methods, depth is estimated from the slope of the azimuthally averaged power spectrum, as demonstrated in Figure 8. These absolute or white depths are at 280 and 500 m in the first area and at 390 and 610 m in the second area. Pilkington et al. (1994) point out that these white depths overestimate true depth. Indeed, it is unlikely that a horizontal source interface would cause a linear section in the power spectrum at all.

Let us now examine relative depth. The difference in slope between areas 1 and 2 is identical in both wavebands and corresponds to a relative difference in depth of 110 m. If we upward continue the spectrum of the paleochannel area by 110 m, it matches the spectrum of the area with outcropping basement. This can be interpreted in such a way that the spectrum of the basement magnetic field is identical in both areas, while the vertical distance to the observation plane is greater by 110 m in the paleochannel area. The difference in slope in a fixed waveband therefore provides an estimate for the relative depth to the basement.

**Depth from the entire spectrum.**—Instead of comparing slopes in fixed wavebands, the depth factor can be analyzed with greater precision by using a model for the entire power spectrum (Figure 9). Here, a self-similar model  $e^{-2zs} s^{-\beta+1}$  is fit to the power spectrum. The best least-squares fit for a constant  $\beta$  provides an estimate of relative basement depth. If the correct value of  $\beta$  is known, then even the absolute depth to basement can be obtained by this approach (Maus and Dimri, 1996). Here, we used  $\beta = 4$ , proposed by Pilkington and Todoeschuck (1995) as the mean scaling exponent of continental crust. Besides explaining the full shapes of the two power spectra, this approach also leads to realistic estimates of absolute depth

from the observation plane to the basement. Subtracting the average sensor clearance of 61 and 56 m gives basement depths below terrain of 59 and 174 m for the outcrop and the paleochannel area, respectively.

**Depth from the variogram.**—The resolution and accuracy of depth estimation can be improved further by shifting the analysis to the space domain and analyzing variograms, as illustrated in Figure 10. Subtracting the sensor clearance from the model depths gives estimates of 12 and 184 m for the depth below terrain. In particular for outcropping basement, the variogram analysis depth of 12 m below terrain is much better than the power spectrum depth of 59 m below terrain (Figure 9). The greater power spectrum depth is probably caused by the smoothing effect of gridding. The grid does not reflect the full ruggedness of the magnetic field over outcropping basement.

**Calibration of depth.**—As described above, the scaling exponent  $\beta$  must be kept at a constant value to be able to resolve depth  $z$ . This corresponds to the assumption of a constant shape (but variable amplitude) of the magnetic power spectrum at basement level. Indeed, the spectral slope method is based on the same implicit assumption. A higher scaling exponent leads to shallower depth estimates and vice-versa. Looking at variogram analysis depth over outcropping basement, we obtain depths close to the sensor terrain clearance for  $\beta = 2.6$ . It is not clear why this value is so much lower than  $\beta = 4$ , which gives a realistic interpretation of the power spectra. Both values should in theory be identical. Possible reasons for the deviation are the smoothness of grids, leading to high power spectrum  $\beta$ , and the subtraction of a linear trend before estimating the variograms, leading to low variogram  $\beta$ .

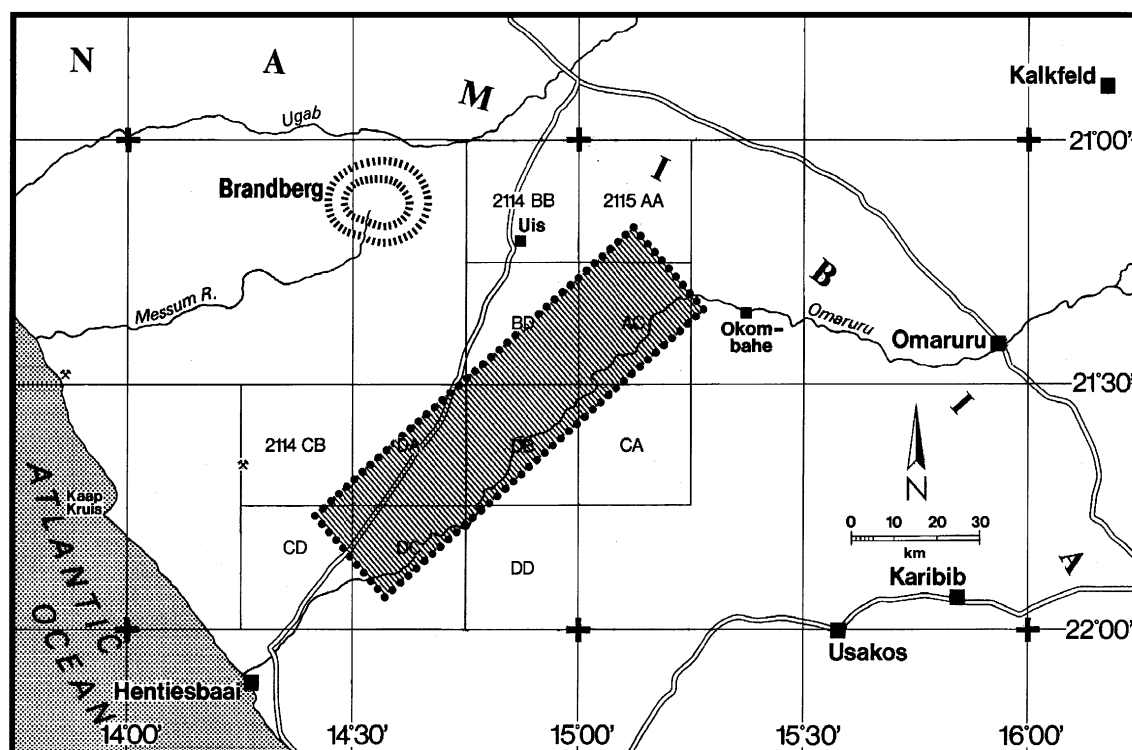


FIG. 4. Location and approximate flight lines of the 100 × 26-km helicopter survey.

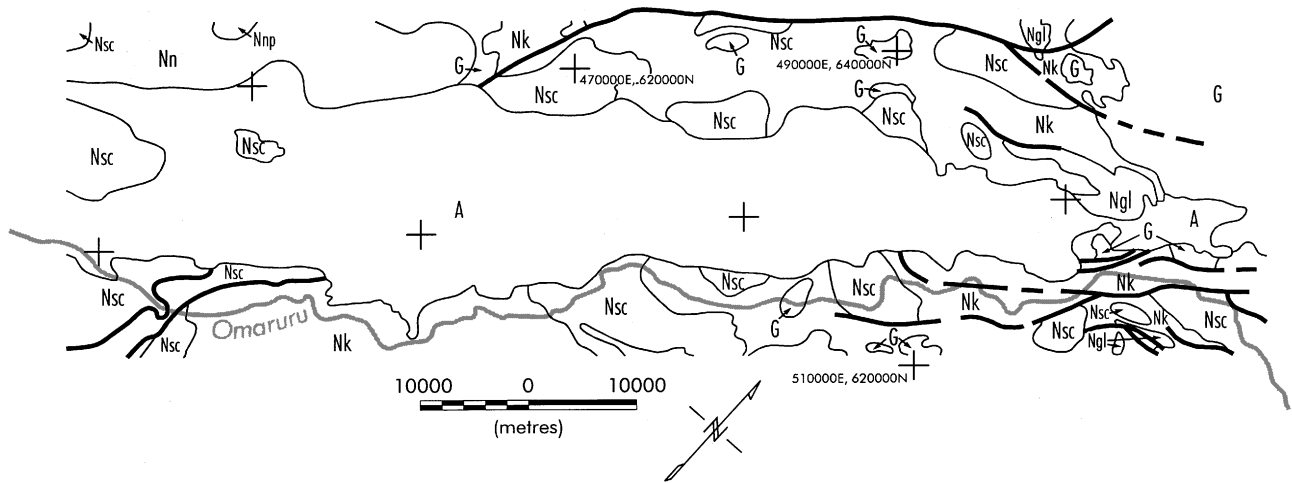


FIG. 5. Geological sketch of the survey area (Miller and Schalk, 1980). (A) Alluvium, (G) granites, (Nsc, Nu, Nk, Nup, Ngl) Damara Orogen Sequence, comprising metamorphosed acid volcanics, mica shists, and gneissic leucogranites.

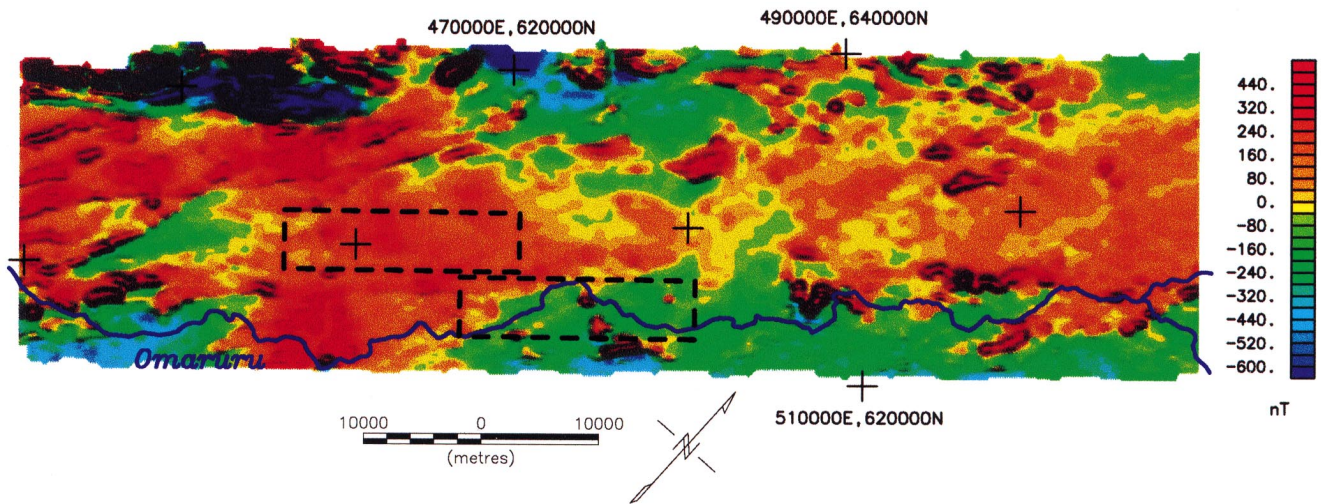


FIG. 6. Shaded  $\Delta T$  total field anomaly map (Paterson and Reeves, 1985) of the survey area with the present Omaruru River. The sample areas are indicated as dashed rectangles.

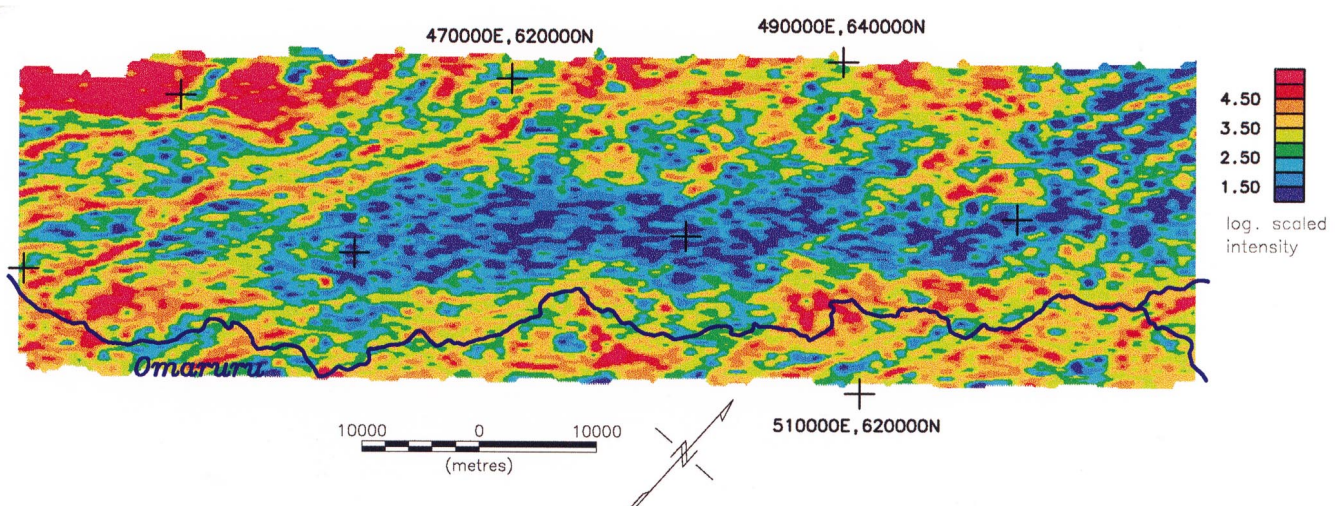


FIG. 7. Map of the intensity  $c_s$ , estimated by variogram analysis from single 500-m along-line sections of  $\Delta T$  data, assuming  $\beta \equiv 2.6$  and  $z$  = terrain clearance. Nonmagnetic alluvial deposits along the center of the area are reflected in low  $c_s$  values.

**Results for the entire survey**

We utilized a scaling exponent of  $\beta = 2.6$  and a window size of  $5 \times 6$  km (along-line  $\times$  across-line) for the variogram analysis (Figure 3). Within this window we calculated the variograms for sections 3 km in length, one every 100 m, and stacked the variograms of the sections along-line as well as across-line. Hence, the resulting variogram is an average of  $21$  (along-line)  $\times$   $7$  (across-line) =  $147$  variograms. This gives a better result than using 5-km variograms and stacking only across-line. We moved the window along-line by 100-m increments. Across-line the window position was incremented by one flight line at a time, corresponding to 1-km intervals.

**Depth versus EM resistivities.**—To some extent, variogram analysis depths below terrain, shown in Figure 11, can be verified by a comparison with measurements from a three-channel

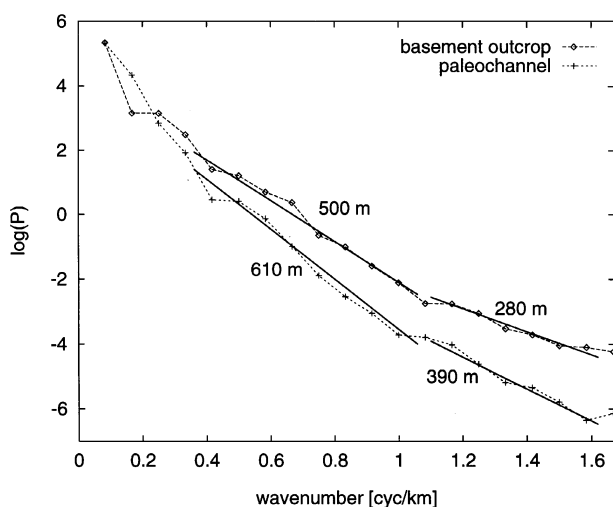


FIG. 8. Power spectra of the two areas indicated in Figure 6 with a spectral slope method interpretation. Note the equal difference in depth of 110 m in both wavebands.

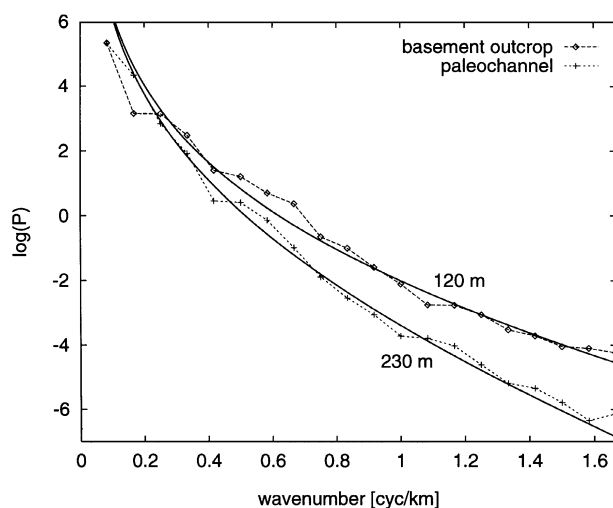


FIG. 9. Same power spectra as in Figure 8 interpreted using a self-similar  $e^{-2\alpha s^{-3}}$  model.

active EM system. The map of  $\rho_4$  from a five-layer inversion (Sengpiel, 1988), shown in Figure 12, provides a horizontal resistivity cross-section at approximately 30 m depth. High resistivity indicates crystalline basement. Low resistivity indicates sediments. Very low resistivities can be caused by saline water or clay. Areas of low resistivity in Figure 12 should therefore coincide with areas of depth greater than about 20 m in Figure 11. All in all, the agreement between the two maps is good. Some structures which are small relative to the  $5 \times 6$  km variogram analysis data window are missing in the variogram analysis depth map. This problem is apparent at the high (right) and low (left) margins of the survey area, where narrow paleochannels are poorly resolved. The wider channel in the center of the study area, on the other hand, is mapped quite accurately.

**Basement relief.**—To display the estimated depth in such a way that paleochannels can be identified, we first subtracted the altitude above mean sea level (a.m.s.l.) of the Omaruru River at the intersection with each flight line from the topography a.m.s.l. along-line. The Omaruru River then flows always at altitude zero, while it actually descends from around 900 m a.m.s.l. in the northeast to around 300 m in the southwest. This relative ground topography is displayed in Figure 13. We then added the negative basement depth estimates, resulting in a basement relief relative to the present-day Omaruru river. The result shown in Figure 14 clearly indicates several paleochannels.

In Figure 15 the corresponding basement relief obtained by an automated spectral slope method is displayed. A window of  $6 \times 6$  km was moved over the magnetic grid of the survey area. The power spectrum was estimated for each window position using a commercially available software package. This software also provides an estimate of three-point slope. By trial and error we found the waveband where relative differences in slope give the best estimates of basement depth. As predicted above, absolute depth below terrain ranging from 550 to 800 m is quite off the mark. Nevertheless, subtracting 550 m leads to a crude but reasonable basement relief.

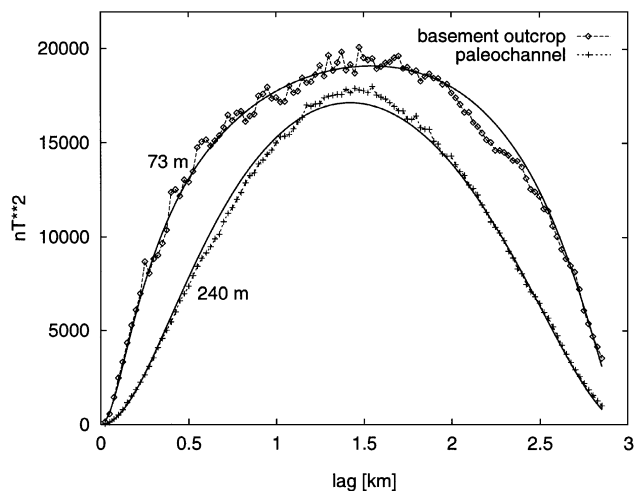


FIG. 10. Modified variograms of the two areas in Figure 6 together with the best-fitting model variograms, indicated as solid lines. For better comparison, the paleochannel variogram is amplified by a factor of 4.0.

**Drilling results.**—Of nine proposed groundwater exploration wells, only three were drilled (BH1, BH2, and BH3 indicated in Figures 11, 13, and 14). After 129 m of gravel, sand, and clay, well BH1 encountered weathered doleritic basement sand, weathered metabasalt at 141 m, and fresh metabasalt at 160 m (variogram analysis prediction 163 m). Well BH2 found basement sand (magnetite, mica, feldspar) at 192 m and hit a granitic basement at 198 m (variogram analysis prediction 182 m). Further downstream, well BH3 found dark basement

sand (magnetite, hornblende) at 96 m and an amphibolitic basement at 110 m (variogram analysis prediction 34 m). Unfortunately, no susceptibilities were measured. All wells were dry.

Drilling results versus predicted depths are summarized in Table 2. Taking into account the 60 m flight altitude of the magnetic sensor, prediction errors for wells BH1 and BH2 are around 10%. In contrast, the prediction for well BH3 is quite off the mark. While variogram analysis depths (Figure 14) correctly indicate the continuation of the central paleochannel, its

**Table 2. Drilled versus predicted basement depths.**

Variable	Well BH1	Well BH2	Well BH3
Lithology	Metabasalt	Granite	Amphibolite
Drilled depth	141 m	198 m	110 m
Variogram analysis depth	163 m	182 m	34 m
Error (off sensor)	11%	6%	45%

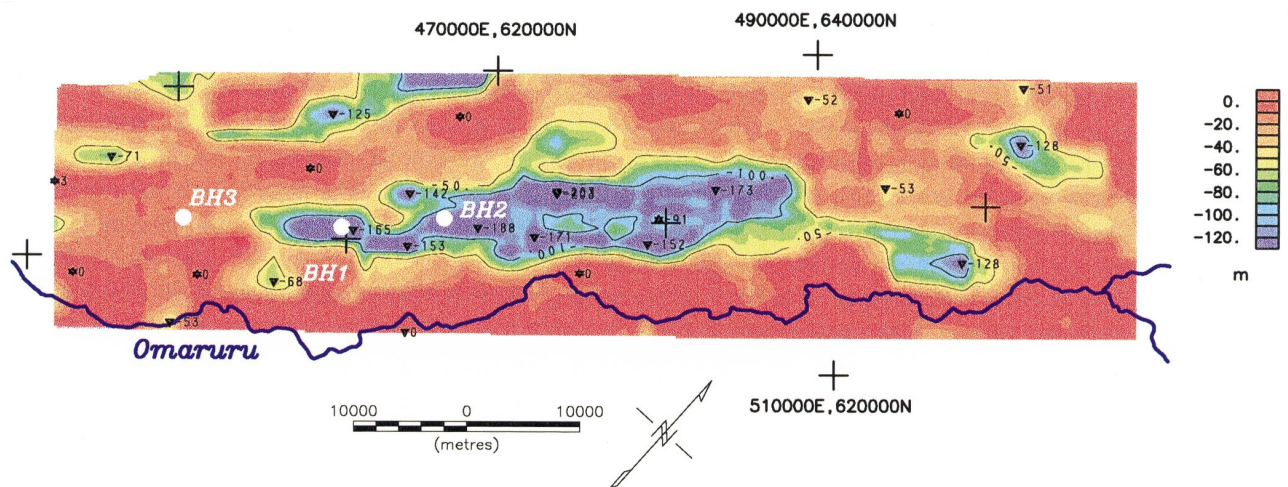


FIG. 11. Variogram analysis depths. BH1, BH2, and BH3 indicate the positions of three groundwater exploration wells.

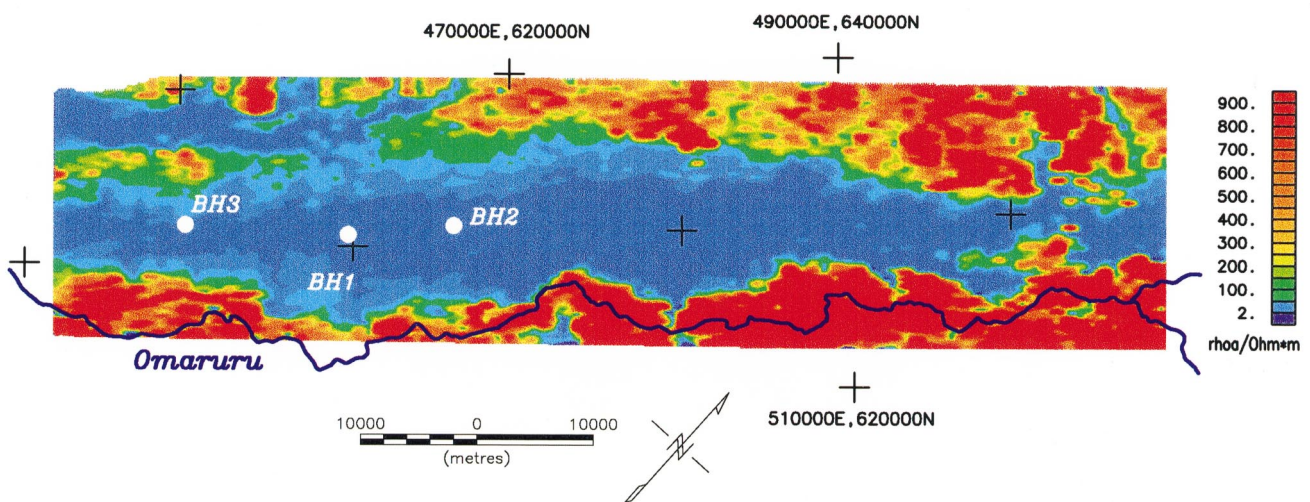


FIG. 12. Map of  $\rho_4$  from a five-layer inversion of measurements from an active three-channel EM system.



depth is grossly underestimated. The channel is probably too narrow here to be resolved accurately by a  $5 \times 6$ -km variogram analysis window.

### CONCLUSIONS

The basement topography of the Omaruru Alluvial Plains has been derived by variogram analysis of an aeromagnetic survey. The method has been designed to make maximum use of the measured data. We have discussed the nonuniqueness of magnetic depth solutions. Besides depth, properties of magnetic mineral distribution and the direction of magnetization influence the smoothness of the magnetic field. Furthermore, steep gradients in basement topography give rise to long-wavelength magnetic anomalies, which are not discernible from deep-seated intrabasement magnetization contrasts. In view of these inherent difficulties of the magnetic method, our result has remarkable resolution and accuracy.

In comparison with spectral slope methods, variogram analysis has these advantages:

- 1) Makes use of the short-wavelength along-line information, which is otherwise lost in gridding. This is the key to reliable depth in shallow sedimentary deposits.
- 2) Has no restriction on the shape of the survey area. Variogram analysis can even process single profiles. In contrast, power spectrum methods require rectangular (usually square) subareas.
- 3) Accounts for the fractal distribution of magnetic minerals by using a self-similar spectral model, leading to more accurate depth estimates.
- 4) Avoids the difficulties (e.g., edge effects) of wavenumber domain power spectrum estimation by using straightforward space domain variograms.

Because of points 1 and 2, variogram analysis has a strong advantage over power spectrum methods in shallow basins. In deep basins, with basement depths larger than flight-line spacing, even grids should contain sufficient high wavenumber information to estimate reliable depth. A power spectrum method could then yield accurate depth, provided the fractal nature of the magnetic source is taken into account, e.g., by using equation (6) as a spectral model. The question remains, however, why the data should be arduously transformed to wavenumber domain when spectral models can be analytically transformed to space domain without loss of information. We argue that a data variogram is easier to estimate and should therefore carry more reliable depth information than a power spectrum, even for surveys of deep basins.

Finally, variogram analysis has an interesting spin-off in terms of a near-surface magnetization intensity map (Figure 7).

Variogram analysis intensity is high when magnetization is high, and vice-versa, simplifying interpretation. Using very short flight-line sections for variogram estimation, maximum use of a short-wavelength along-line signal can be made. This amplifies small structural features that are usually lost in gridding. Variogram analysis intensity maps could therefore be helpful in detecting weak intrabasinal signatures from high-resolution aeromagnetic data in petroleum exploration.

### ACKNOWLEDGMENTS

We thank Ursula Noell for providing the drilling results. Helpful discussions with Mike Leeder, Andy Jackson, and Alan Reid, as well as the detailed reviews by David Chapin, Afif Saad, Jeff MacQueen, and Harold Yarger, are gratefully acknowledged.

### REFERENCES

- Alexander, J., Bridge, J. S., Leeder, M. R., Collier, R. E. L., and Gawthorpe, R. L., 1994, Holocene meander-belt evolution in an active extensional basin, southwest Montana: *J. Sed. Res.*, **B64**, no. 4, 542–559.
- Bittner, A., Sengpiel, K. P., Siemon, B., Röttger, B., Voß, W., and Pielawa, J., 1994, Exploration drilling proposal, **B-II**: BGR Archives No. 112 775, Hannover.
- Gregotski, M. E., Jensen, O. G., and Arkani-Hamed, J., 1991, Fractal stochastic modeling of aeromagnetic data: *Geophysics*, **56**, 1706–1715.
- Hahn, A., Kind, E. G., and Mishra, D. C., 1976, Depth estimation of magnetic sources by means of Fourier amplitude spectra: *Geophys. Prosp.*, **24**, 287–308.
- Leeder, M. R., and Alexander, J., 1987, The origin and tectonic significance of asymmetrical meander belts: *Sedimentology*, **34**, 217–226.
- Maus, S., 1999, Variogram analysis of magnetic and gravity data: *Geophysics*, **64**, 775–783.
- Maus, S., and Dimri, V. P., 1995, Potential field power spectrum inversion for scaling geology: *J. Geophys. Res.*, **100**, 12605–12616.
- 1996, Depth estimation from the scaling power spectrum of potential fields?: *Geophys. J. Internat.*, **124**, 113–120.
- Miller, R. M., and Schalk, K. E. L., 1980, Geological map of Namibia, scale 1:1,000,000: Namibia Geological Survey.
- Nawrowski, J., 1993, An overview of the hydrogeology in the Omaruru Alluvial Plains (OMAP): Geohydrology Division, Windhoek, Namibia, Dept. of Water Affairs, Interoffice Memorandum.
- Paterson, N. R., and Reeves, C. R., 1985, Applications of gravity and magnetic surveys: The state-of-the-art in 1985: *Geophysics*, **50**, 2558–2594.
- Pilkington, M., and Todoeschuck, J. P., 1993, Fractal magnetization of continental crust: *Geophys. Res. Lett.*, **20**, 627–630.
- 1995, Scaling nature of crustal susceptibilities: *Geophys. Res. Lett.*, **22**, 779–782.
- Pilkington, M., Todoeschuck, J. P., and Gregotski, M. E., 1994, Using fractal crustal magnetization models in magnetic interpretation: *Geophys. Prosp.*, **42**, 677–692.
- Sengpiel, K.-P., 1988, Approximate inversion of airborne EM data from a multi-layered ground: *Geophys. Prosp.*, **36**, 446–459.
- Spector, A., and Grant, F. S., 1970, Statistical models for interpreting aeromagnetic data: *Geophysics*, **35**, 293–302.
- Yaglom, A. M., 1986, Correlation theory of stationary and related random functions, **1**: Springer-Verlag New York, Inc.